Measurement 181 (2021) 109561

Contents lists available at ScienceDirect

Measurement

journal homepage: www.elsevier.com/locate/measurement

A general methodology to determine natural radionuclides by well-type HPGe detectors

A. Barba-Lobo *, E.G. San Miguel, R.L. Lozano, J.P. Bolívar

Department of Integrated Sciences, Center for Natural Resources, Health and Environment (RENSMA), University of Huelva, 21071 Huelva, Spain

ARTICLE INFO

Keywords:
Gamma–Alpha-particle spectrometry
Well-type Ge detectors
Efficiency calibration
Self-absorption correction
Anti-Compton system
NORM

ABSTRACT

This work aims to determine natural radionuclides (^{210}Pb, ^{228,226}Ra, ^{234,228}Th and ^{40}K) in NORM samples by well-type HPGe detectors because they are of vital importance in studies on environmental samples. For this, a novel methodology has been developed, based on obtaining a general function for the full-energy peak efficiency (*FEPE*) versus the sample apparent density and composition, keeping the sample height constant. To obtain the general *FEPE* function, a calibration in efficiency has been accomplished using certified standards provided by IAEA (RGU-1 and RGTh-1), and KCl. Besides, different self-absorption correction functions were compared for cylindrical geometry, where chemical compositions need to be known. Then, a study on using an anti-Compton system was done, getting a lower detection limit and allowing to propose gamma spectrometry as an alternative technique to alpha-particle spectrometry. Finally, the followed methodology to calculate the *FEPE* was subjected to internal and external validations, checking its validity range.

1. Introduction

In the last decades, the natural radionuclides such as ^{210}Pb, ^{228,226}Ra, ^{234,228}Th and ^{40}K are being of great interest due to their wide usage in many environmental fields. The knowledge and use of these radionuclides can be very useful in covering different problems present in the environment, such as the calculation of residence times of atmospheric aerosols [1]. Another example is marine scavenging where ^{234}Th is widely used [2]. ^{210}Pb determination is also interesting in order to date sediments or assess the erosion of a material [3,4].

When a material contains important concentrations of natural radionuclides, it has to be considered as a NORM sample (Naturally Occurring Radioactive Material) (for further information about NORM samples, see [5–10]). There are many industries that produce, for example, metals or fertilizers which generate industrial wastes with high concentrations of natural radionuclides. Consequently, spectrometric techniques need to be employed in order to assess the radiotoxicity to which the workers are exposed. Furthermore, materials related to building construction must be subjected to a radiological control [11].

On the other hand, in order to determine natural long-lived radionuclides by gamma spectrometry, an efficiency calibration of the detectors is necessary. Nowadays the calibration of detectors by Monte Carlo simulations has become generalized (for further information about Monte-Carlo simulations carried out in HPGe detectors, see [12–16]). Thus, there are many cases for which old detectors are not characterized, and the laboratories have to send them into the factory to carry out the characterization procedure, involving high costs for the characterization and the new Monte Carlo software, and needing to wait some time without gamma measurements.

In contrast to Monte Carlo simulations, well-type Ge detectors can be calibrated relatively quickly and using calibration standards that do not imply so high costs. Besides, they have a high absolute efficiency which is about 40 % at low energies, that is, $E_\gamma \leq 150$ keV (where E_γ is the gamma emission energy). That efficiency value is approximately four times higher than the one obtained for any another coaxial detector for that same energy range, being this very important since self-absorption effects are more relevant for low energies. This agrees with many studies carried out on self-absorption corrections [3,17–24]. Regarding corrections related to self-absorption effects, in [25] a correction model was proposed, which is usually used in the case of coaxial well-type detectors. In the present study, the previous model has been employed and its validity has been checked, comparing it with other possible functions.

Furthermore, there are different techniques that are used to determine long-lived natural radionuclides, such as alpha-particle spectrometry with semiconductor detectors, Inductively Coupled Plasma Spectroscopy (ICP), Neutron Activation Analysis (NAA), Liquid

* Corresponding author.
E-mail address: alejandro.barba@dci.uhu.es (A. Barba-Lobo).

https://doi.org/10.1016/j.measurement.2021.109561
Received 1 January 2021; Received in revised form 5 April 2021; Accepted 6 May 2021
Available online 15 May 2021

Scintillation Counting (LSC) and Gamma-ray spectrometry. The former requires tedious procedures in the case of ^{228}Ra and ^{226}Ra determinations [26,27]. Then, regarding the ICP technique, it is necessary to use chemical isolation methods in order to determine radionuclides [28,29]. On the other hand, when employing the LSC technique, it is more recommendable to use it in the cases of the radionuclides whose half-lives are not very high because the frequency of the decay is proportional to the half-life [30,31]. Regarding the NAA, a nuclear reactor would be required in order to apply this technique and, consequently, a very significant cost and power supply would be needed [32,33]. For these reasons, gamma spectrometry has been proposed in this study as an alternative sensitive radiometric technique and with low cost per sample. In the case of alpha-particle spectrometry, since this technique is characterized by having low detection limits for most of the natural radionuclides, in this work it has been carried out an in-depth study related to the advantages and disadvantages of using an anti-Compton system.

Considering all the topics previously exposed, this work is focused on developing a novel methodology, which is explained in Materials and methods Section, to obtain a general *FEPE* function for determining natural long-lived radionuclides in the case of using coaxial well-type germanium detectors. Besides, an original study about benefits and drawbacks of using an anti-Compton system has been done considering several kinds of NORM samples, as well as a comparison between alpha-particle and gamma spectrometric techniques has been made.

2. Materials and methods

2.1. Materials

For this study, a coaxial well-type HPGe detector (model GCW3023) was employed, where HPGe means high purity germanium. This detector has a relative efficiency of 34.8 % in relation to a NaI (Tl) detector with an active area of 3″ x 3″, as well as a full width at half-maximum (FWHM) of 1.33 keV at 122 keV (^{57}Co) and 2.04 keV at 1332 keV (^{60}Co), and a peak/Compton ratio of 56.2/1. Besides, it has a well depth of 40 mm and an active volume of 180 cm^3. The detector was coupled to a multichannel analyzer and shielded with 10 cm thick Pb, using Genie 2000 as the software to generate the spectra. In order to avoid interferences from Pb X-ray, a 2 mm thick layer of Cu was placed between the Pb shield and the detector.

With regard to the anti-Compton system used in this study, it consists of seven NaI (Tl) detectors which are connected between them and they are placed around the well-type HPGe detector to properly reduce the Compton continuum. It is necessary to clarify that this system is called "anti-Compton" system, however its function is to eliminate all the particles detected in coincidence. In the case of the photons, they suffer either photoelectric effect or Compton scattering, the second phenomenon being the one that the majority of the photons suffer. For this reason, this system is called anti-Compton system.

In order to obtain the experimental efficiency values of the detector in the calibration matrix, certified standards provided by the IAEA (International Atomic Energy Agency) were employed, being their codes RGU-1 and RGTh-1. These two calibration samples contain natural radionuclides belonging to ^{238}U- and ^{232}Th-series, where the reference values for activity concentration and densities are 4940 ± 15 Bq kg^{-1} and 3250 ± 45 Bq kg^{-1}, and 1.63 ± 2 g cm^{-3}, respectively, with uncertainties given at 1 sigma level. Both certified standards are mainly composed by SiO_2, which was used to dilute U (7.09 %) and Th (2.89 % Th and 219 ppm of U) ores whose codes are BL-5 and OKA-2, respectively. On the other hand, high purity KCl was also used as a calibration standard for ^{40}K, where its reference activity concentration was obtained by the relation established by the IAEA, that is, 1% of natural K → 313 Bq kg^{-1} of ^{40}K. (See [34,35] for further information about the characteristics of RGU-1, RGTh-1 and RGK-1). For further information about chemical compositions of the calibration samples used in this study, see Table A.14 in Supplementary Material.

On the other hand, several real samples have been chosen in order to apply the methodology proposed in this study. Therefore, NORM samples were chosen due to their wide variety of chemical compositions and densities. Consequently, a proper validation procedure of the followed methodology can be carried out. So, the real samples selected were the following, which have been chosen because of having very different densities and compositions. They have been divided into two groups (non-certified and certified samples): 1. Non-certified samples: Ilmenite, Industrial waste (Scale-1), Phosphate Rock-1 (PR-1), Distilled water; 2. Certified samples: Soil (IAEA-326), K_2SO_4 (RGK-1), Phosphogypsum (IAEA-434), Phosphogypsum used in a CSN/CIEMAT Inter-Comparison exercise (CSN-PG), Phosphate Rock-2 (PR-2). See Table A.14 in Supplementary Material to know chemical compositions and apparent densities of all the real samples selected in this work. Regarding CSN and CIEMAT, they are the acronyms for the Spanish Nuclear Safety Council ("Consejo de Seguridad Nuclear") and the Centre for Energy, Environment and Technology Research ("Centro de Investigaciones Energéticas, Medioambientales y Tecnológicas"), respectively.

2.2. Methods

Regarding the calibration procedure in efficiency, cylindrical plastic vials were used as containers whose height (h), radius (a) and volume (V) were 3.50 ± 0.02 cm, 0.670 ± 0.010 cm and 4.94 ± 0.15 cm^3, respectively. Then, since the calibration samples were prepared at the same height, h, RGU-1 and RGTh-1 standards were mixed with other kinds of samples to get cover a density range as wide as possible. These other samples were PbS and activated carbon.

About the mixtures made to obtain standards whose densities were high, that is, between PbS and RGU-1/RGTh-1, a total of 13 mixtures were prepared in both cases, where the proportion of both standards varied from 10 % to 97 %. In this case, a code was employed in order to identify each mixture. Therefore, STi-U and STi-Th were the codes for mixtures made with RGU-1/RGTh-1 and PbS, respectively, being "i" the proportion of the standards in each one of the mixtures (see Tables A.1 and A.2, respectively, in Supplementary Material). On the other hand, with regard to the mixtures carried out in order to lower the density of the standards, that is, between activated carbon and RGU-1/RGTh-1, a total of 3 mixtures were made for each one of the standards. Analogously to the previous case, a code was used to identify each mixture, being in this case Ci-U and Ci-Th, where "i" is the proportion of the standards in each mixture (see Tables A.6 and A.7, respectively, in Supplementary Material).

Apart from the mixtures of the standards (RGU-1 and RGTh-1) with PbS and activated carbon previously described, 9 calibration samples were prepared for both standards varying the grade of compaction of each one of them. In this case, the code used to identify each calibration sample was RGUi and RGThi, where "i" was ranged from 1 to 9, increasing the compaction grade as "i" increases (see Tables A.3 and A.4, respectively, in Supplementary Material). Therefore, a total of 25 calibration samples were prepared for RGU-1 and RGTh-1 in order to carry out the calibration in efficiency. On the other hand, in the case of KCl calibration standard, this was dissolved in water and, consequently, K concentration was varied getting 9 calibration samples. For these calibration samples, the identifier code was K-i, where "i" was ranged from 1 to 9, increasing the K concentration as "i" increases (see Tables A.5 in Supplementary Material).

Besides, it is necessary to clarify that the relative uncertainties related to the activities of ^{238}U, ^{232}Th and ^{40}K, that is, A(^{238}U) (Bq), A(^{232}Th) (Bq) and A(^{40}K) (Bq), respectively, which can be found in Tables A.1–A.7, can be approximated by the relative uncertainties corresponding to the reference activity concentration values. This is possible because in order to proceed with the A(^{238}U), A(^{232}Th) and A(^{40}K) calculations, there are only two main contributions, that is, the reference activity concentrations and the masses of each standard

contained in the vials, where the relative uncertainties related to the latter contribution can be completely neglected.

Once all the calibration samples were prepared, experimental full-energy peak efficiencies calculated in the calibration matrix (ε_{exp}) were obtained fixing the gamma emission energy (E_γ) and varying the calibration sample density (ρ) or varying the calibration sample mass (m) since the volume of sample container is fixed. After obtaining the experimental efficiencies, it was necessary to calculate another kind of full-energy peak efficiency, ε_0^{exp}, which represents the experimental detector efficiency calculated in the matrix of a sample whose mass tends to zero. These calculations were possible due to the relation between both kinds of efficiencies, that is

$$\varepsilon_{exp} = f\varepsilon_0^{exp} \tag{1}$$

where f is the self-absorption correction factor, having used in this case the one proposed in [25]. The f factor is necessary to be employed in order to consider the attenuation effects when the sample mass (or density) is different from zero.

Consequently, for all the gamma energies belonging to the radionuclides that are contained in RGU-1 and RGTh-1 standards, 25 values of ε_{exp} were obtained, that is, a value for each calibration sample prepared. Analogously to ε_{exp} values obtained in the cases of RGU-1 and RGTh-1 standards, 9 values of ε_{exp} were calculated for KCl standard. See Tables A.8, A.9 and A.10 in Supplementary Material for further information about ε_{exp} values calculated in the cases of RGU-1, RGTh-1 and KCl standards, respectively, as well as the E_γ values selected to carry out the calibration in efficiency and their respective emission probabilities (P_γ). In those three tables, each ε_{exp} value is associated to a ηm value, where η and m are the mass attenuation coefficient and mass of each calibration sample that has been prepared. Once the ε_0^{exp} values were obtained for each energy, an average ε_0^{exp} value, ε_0, was determined for each one of these energies (see Table A.11 in Supplementary Material).

3. Results and discussion

This Section has been divided into five subsections: Calibration in efficiency, self-absorption correction functions, an in-depth study on using anti-Compton system (including applications to both the detection limit calculations and gamma spectrometry versus alpha-particle spectrometry), internal and external validations of the methodology followed in this work and a proposed method to determine ^{226}Ra in phosphogypsum and aqueous samples.

3.1. Obtaining of the full-energy peak efficiencies (FEPEs) in the calibration matrices

The experimental *FEPEs* (ε_{exp}) in the calibration samples for a given energy E_γ, is obtained through the following equation:

$$\varepsilon_{exp}(E_\gamma, m) = \frac{G - B - F - I}{maP_\gamma t} = \frac{N}{maP_\gamma t} \tag{2}$$

where G, B, F, I and N are the gross counts, the continuum Compton, the background due to the environmental conditions of the laboratory, interference terms and the net counts, respectively. Then, P_γ is the gamma emission probability, which were taken from [36] a and m are the activity concentration and mass of the samples (in this case, calibration standards), respectively, t the counting time. Only gamma emissions without interferences have been selected so $I \sim 0$.

Once the ε_{exp} values have been calculated by Eq. (2), it is possible to obtain ε_0^{exp} by Eq. (1). Furthermore, it is necessary to know the function employed to quantify the self-absorption corrections. In this case, it has been used the correction function proposed in [25], which is given by the following expression:

$$f(x^2) = 2\exp(-kx^2)\left[(kx^2)^{-1}\sinh(kx^2) - (kx^2)^{-2}(\cosh(kx^2) - 1)\right] \tag{3}$$

where $x^2 = \eta m$, being m and η the sample mass and mass attenuation coefficient, respectively, η being related to the sample linear attenuation coefficient (μ) and density (ρ) by $\eta = \mu/\rho$. Then, k is the geometric parameter characterizing the dimensions of the sample, which is given by $k = (\pi ah)^{-1}$, where a and h are the radius and height of the sample container used in the procedure of efficiency calibration, respectively, and whose values were previously mentioned in Materials and methods Section. In order to obtain the η value corresponding to a sample, it was necessary to use the Bragg's additivity law, which says that $\langle\eta\rangle = \sum_i x_i\eta_i$, where x_i and η_i are the proportion and mass attenuation coefficient of each major chemical element "i" contained in the sample, respectively, and $\langle\eta\rangle$ is the mass attenuation coefficient of the sample (see [17,24,37] for further information about Bragg's additivity law).

In Fig. 1, ε_{exp} for the calibration samples have been plotted as a function of x^2 (where η values for each chemical element were taken from [38]) for each specific gamma energy selected in the calibration procedure. As can be seen from Fig. 1, the majority of the *FEPE* curves show a similar general behavior, that is, ε_{exp} values decrease as energy increase and form curves that are quite parallel similar to each other. However, there are some efficiency curves which do not follow that tendency, occurring this at the following energies: 46 keV, 583 keV, 609 keV, 768 keV and 1120 keV. For 46 keV, the reason of a different behavior is the self-absorption effects which are more relevant for lower energies. On the other hand, for the other three energies, the reason would be related to true coincidence summing effects (TCS), being summing-out effects for these three energies [39–41]. Considering these motives, it is possible to understand why the behavior of those energies is so different compared with the other ones.

Furthermore, from Fig. 1 it can be observed that ε_{exp} uncertainties (at 1 sigma level) are relatively small. Numerical values for ε_{exp} and uncertainties for each ηm value are shown in Tables A.8–A.10. In these tables, ε_0^{exp} values are also shown. Therefore, from all the ε_0^{exp} values obtained for a same energy, an average ε_0^{exp} value (ε_0) has been determined for each gamma energy. These ε_0 values for each specific energy can be found in Table A.11 in Supplementary Material. In Tables A.11, it can be seen that the uncertainties of ε_0 values are relatively small. This occurs in this way because they have been determined by propagation of uncertainties, so the uncertainties decrease as the number of experimental data increase. On the other hand, in order to look for a relationship between ε_0 and E_γ, $\ln(\varepsilon_0)$ versus $\ln(E_\gamma/E_0)$, where $E_0 = 1$ keV, have been plotted in Fig. 2 for high energy values, that is, $>150E_\gamma$ keV. From Fig. 2 it can be observed a clear linear tendency excepting for 583 keV, 609 keV, 768 keV and 1120 keV which suffer summing-out effects as it was previously mentioned. Discarding these energies, a linear fitting of $\ln(\varepsilon_0)$ versus $\ln(E_\gamma/E_0)$ has been accomplished obtaining a relative average residue of 7.5 %.

To calculate the relative average residue ($\langle$Res$\rangle$ (%)), the following equation was employed:

$$\langle Res\rangle = \sqrt{\frac{1}{s-1}\sum_{i=1}^{s}\left[100\left(\frac{y_{fit}^{(i)}}{y_{exp}^{(i)}} - 1\right)\right]^2} \tag{4}$$

where $y_{exp}^{(i)}$ and $y_{fit}^{(i)}$ are the values obtained experimentally and the ones obtained by a fitting function for a magnitude y, respectively, s being the number of experimental data.

3.2. Comparison between different possible self-absorption correction functions

In the calculations of ε_{exp} values, which have been shown in Tables A.8–A.10, we have assumed that Eq. (3) is completely valid in

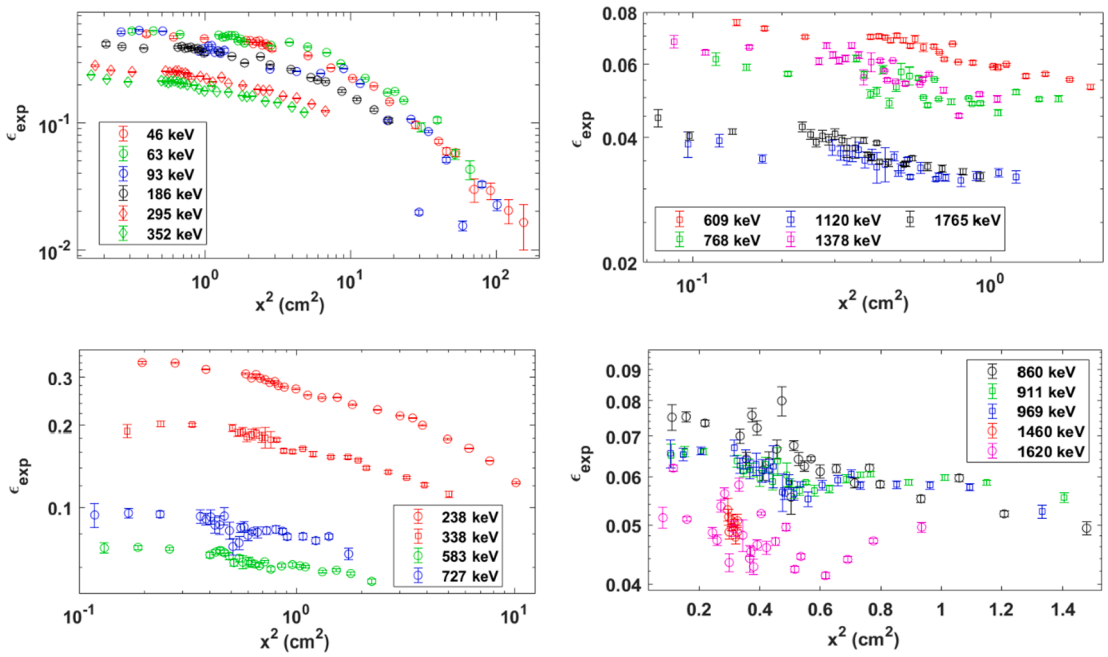

Fig. 1. Experimental efficiency values (ε_{exp}) plotted versus x^2, where $x^2 = \eta m$, for each gamma emission energy of the radionuclides belonging to the ^{238}U- and ^{232}Th-series and ^{40}K, and varying the density of the RGU-1 (mixed with PbS), RGTh-1 (mixed with PbS) and KCl (dissolved in water) standards.

order to correct self-absorption effects in the case of the samples measured by a well-type detector. Therefore, in this Section it has been done a test about the Eq. (3) validity, as well as a comparison between corrections given by Eq. (3) and other possible functions that provide a good fit of ε_{exp} values. For this, three kinds of functions (*Function-i*, where $i = 1, 2, 3$) have been selected in order to fit the ε_{exp} values that have been shown in Fig. 1. The parameters to be adjusted are designed by F_{ij} (parameter j from *Function-i*). These three functions are given by the following equations, which depend on the variable $x^2 = \eta m$, where η and m are the mass attenuation coefficient and the mass of the selected sample, respectively:

$$Function-1: \quad \varepsilon^{(1)} = \varepsilon_0(E_\gamma) f(kx^2) = F_{11} f(F_{12}x^2) \tag{5}$$

where $F_{11} = \varepsilon_0(E_\gamma)$ are the efficiency values at each energy, which have been shown in Tables A.11, and $f(kx^2)$ is the function given by Eq. (3), being $F_{12} = k$.

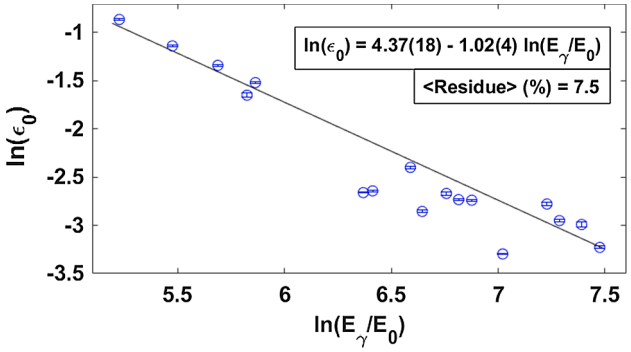

Fig. 2. Fitting of ε_0 values versus $ln(E_\gamma/E_0)$ at high energies, considering the gamma emissions of the radionuclides belonging to the ^{238}U- and ^{232}Th-series, as well as ^{40}K, and calculation of ⟨Res⟩ values resulted from this fitting.

$$Function-2: \quad \varepsilon^{(2)} = 2F_{21}\exp\left(-F_{22}x^2\right)\left[\left(F_{23}x^2\right)^{-1}\sinh\left(F_{24}x^2\right) - \left(F_{25}x^2\right)^{-2}\left(\cosh\left(F_{26}x^2\right) - 1\right)\right] \tag{6}$$

where F_{2j} are the parameters resulted from fittings provided by *Funtion-2*, being j ranged from 1 to 6.

$$Function-3: \quad \ln\left(\varepsilon^{(3)}\right) = \sum_{j=1}^{3} F_{3j}\ln\left(x^2/x_0^2\right)^{j-1} \tag{7}$$

where F_{3j} are the parameters resulted from fittings provided by *Funtion-3* and $x_0^2 = \eta_0 m_0 = 1$ cm^2 is introduced for the argument of the functions to be dimensionless.

In order to compare the fittings of ε_{exp} provided by those three functions, the most relevant gamma emission from ^{238}U- and ^{232}Th-series radionuclides were considered. Fig. 3 shows the fitting of ε_{exp} versus ηm values for the different functions. The ε_{exp} values are the same that the ones shown in Tables A.8, A.9, provided by each function for each one of the main gamma energies of the ^{238}U- and ^{232}Th-series. In Fig. 3 note that the fittings provided by *Function-1* agree very well with experimental data for all the emission energies except in the cases corresponding to low energies, that is, 46 keV and 63 keV, particularly for high ηm values when attenuation effects are more significant.

Moreover, in Tables A.12 (in Supplementary Material) it can be found the parameters resulted from the fittings provided by the three functions, as well as the relative average residues obtained for each fitting for a given energy. Regarding the fittings carried out in this Section as well as all the other sections, they were compared statistically by finding their confidence intervals using MATLAB (see [42] for further information about the algorithms used to provide the fittings). In Tables A.12 it can be observed that the residues provided by *Function-1*

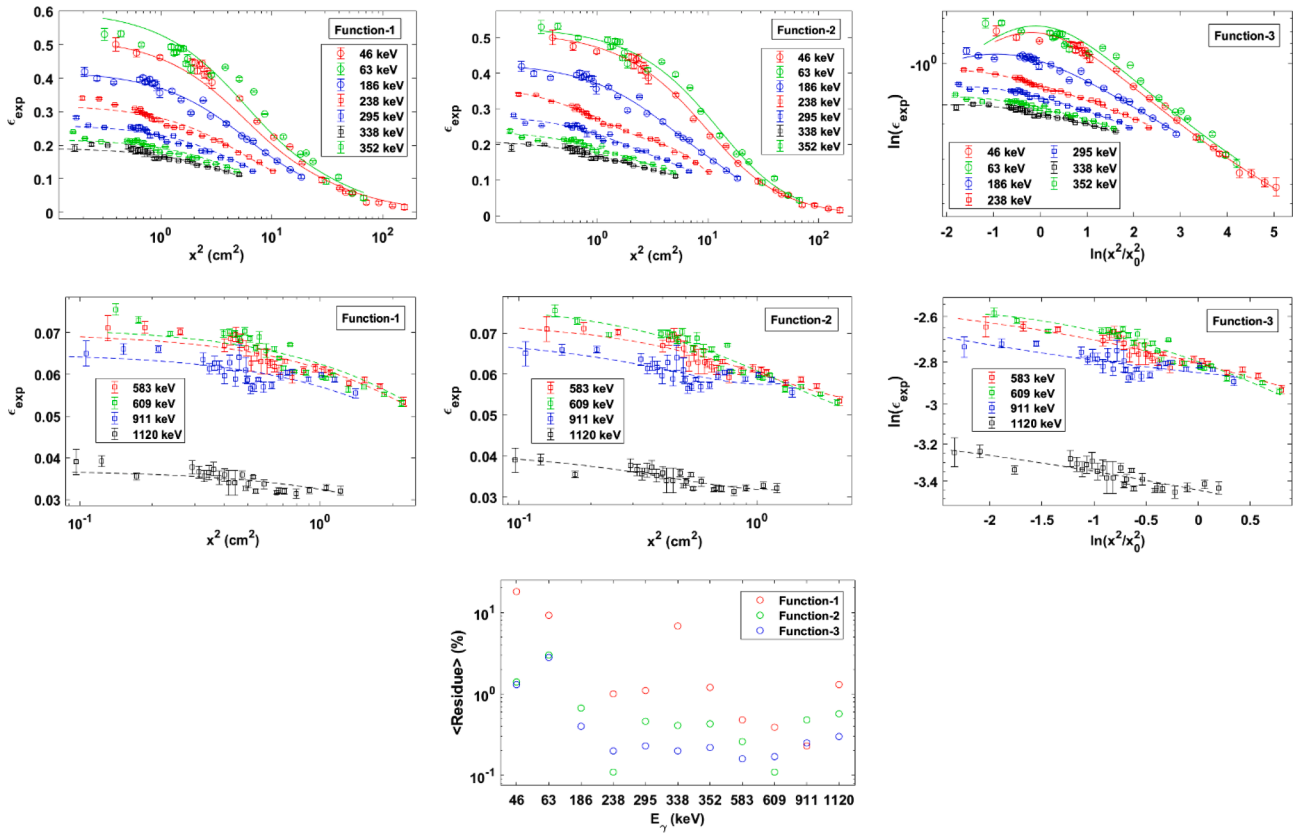

Fig. 3. Comparison between the fittings done by different functions (*Function-i*, with "i" = 1, 2, 3) for ε_{exp} versus x^2 (in the cases of *Function-1* and *Function-2*), and for $\ln(\varepsilon_{exp})$ versus $\ln(x^2/x_0^2)$ (in the case of *Function-3*), being $x^2 = \eta m$ and $x_0^2 = \eta_0 m_0 = 1$ cm^2.

are much higher at low energies (18 % and 9.2 % at 46 keV and 63 keV, respectively) than at higher energies. This is due to the fact that one of requirements for validity of Eq. (3) is that photons must travel parallel to the radial axis of the sample container and the sample itself (cilindrycal geometry). Therefore, for samples whose densities and average atomic numbers, $\langle Z \rangle$, are very high (compared, for example, with the $\langle Z \rangle$ value of a soil, that is, $\langle Z \rangle \sim 10.6$), the previous requirement will not be fulfilled. As attenuation increases, the angle formed by the traveling direction of photons and the radial axis differs more and more from zero, this being especially true for low energy photons. Consequently, the function given by Eq. (3) fails to correct self-absorption effects in well-type detectors for high density and high $\langle Z \rangle$ samples.

On the other hand, in Fig. 3 it can also be observed the fittings of ε_{exp} values versus ηm values provided by *Function-2* and *Function-3*, where in the case of *Function-3*, the fittings have been carried out for the logarithms of ε_{exp} and ηm. Thus, for both functions it can be seen a good agreement between the fittings and experimental data. The parameters and relative average residues resulted from these fittings are shown in Tables A.12. As it can be seen from Tables A.12 the residues related to the fittings provided by *Function-2* are lower than one excepting for 46 and 63 keV with 1.4 and 3 % respectively. This also occurs for the results provided by *Function-3*. The relative average residues have been shown in Fig. 3. In this graphic, it can be note that the great majority of the fittings provided by *Function-1* are better as E_γ increases, being most of these residues less than 1.3 %. In that same graphic, it is possible to see that the residues obtained in the cases of *Funtion-2* and *Function-3* ranged from 0.1 % to 3.0 %.

3.3. Study on advantages and disadvantages about using an anti-Compton system

One of the main objectives of using an anti-Compton system is to reduce the Compton continuum, and consequently, get higher efficiencies. Thus, given that the operation of this system consists in eliminating counts generated by photons that have been detected in coincidence by NaI (Tl) detectors, there might be some energies for which the anti-Compton system does not work properly. This means that the system could eliminate counts that should not be neglected. In this Section, a comparison between the counting rates obtained with the anti-Compton system switched on (n^a) and off (n) has been made. This comparison has been done with samples covering a wide range of densities and compositions.

In Fig. 4, it can be found the ratios of n^a and n plotted for the following nine samples: Scale-1, IAEA-326, Ilmenite, RGU-1, RGTh-1, RGK-1, RGU-1 + 70 % PbS, RGTh-1 + 70 % PbS and RGK-1 + 70 % PbS. Those ratios have been plotted at 46 keV, 63 keV, 186 keV, 238 keV, 295 keV, 338 keV, 352 keV, 583 keV, 609 keV, 911 keV, 1120 keV and

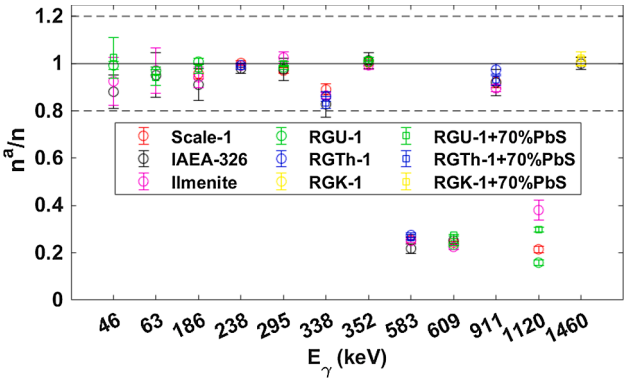

Fig. 4. Comparison between the counting rates obtained for several types of samples, with the anti-Compton system switched on and off.

1460 keV.

From Fig. 4, it can be seen that the anti-Compton system is working properly for many energies since most ratios are close to 1, obtaining a maximum deviation of approximately 15 %. However, there are three energies that clearly differ from the others: 583 keV, 609 keV and 1120 keV. As it was previously commented, these energies have summing-out effects, and consequently, for these energies, emissions of photons in cascade are being occasioned. If two photons are emitted in cascade it is possible that one of them could be scattered by Compton effect whereas the other interact by photoelectric effect. In this situation, the anti-Compton system is eliminating counts that should not be eliminated, since it is eliminating counts generated by photons suffering photoelectric effect, which contribute to the full-energy peak efficiency. Consequently, for 583 keV, 609 keV and 1120 keV, the counting rates obtained with the anti-Compton system on are lower than the ones obtained with this system off. Besides, there are many studies indicate that the true coincidence summing effects (TCS) are more significant in the well-type detectors [40,43,44] so in these detectors, it is easier to check the mistakes made by the anti-Compton system for gamma emissions in cascade.

On the other hand, in Fig. 4 it is also possible to note that n^a/n ratios do not depend on the chemical compositions of the samples chosen for this study. For this reason, samples whose densities and compositions are so different from each other, have been selected. The fact that n^a/n values do not depend on the kind of sample is very understandable and it is explained below. If we take Eqs. (1) and (2) and consider that all the variables present in these equations are the same except ε_{exp} when using or not using the anti-Compton system, the self-absorption correction factor will be cancelled after dividing n^a between n. This is consistent because in both cases (with and without anti-Compton system), the measured sample is the same and, therefore, the correction given by the self-absorption factor is also the same. This is very useful because in the cases of 583 keV and 609 keV, n^a can be corrected perfectly by the n/n^a ratio, getting to solve the problem occasioned by the anti-Compton system for those two energies.

Nevertheless, in Fig. 4 it is easy to see that there is only one energy which does not follow the same tendency than the others, being this energy 1120 keV. In this case, the self-absorption effects affecting the counting rate with the anti-Compton system on (n^a) are different from those affecting the counting rate with the anti-Compton system off (n). This fact can be explained because 1120 keV is characterized by having summing-out effects, that is, $E_\gamma^{(3)} = E_\gamma^{(1)} + E_\gamma^{(2)}$, where $E_\gamma^{(3)}$ is 1120 keV and $E_\gamma^{(1)}$ and $E_\gamma^{(2)}$ are the energies corresponding to two other photons. Therefore, if $E_\gamma^{(1)}$ or $E_\gamma^{(2)}$ were energies corresponding to the low energy region, and considering that the anti-Compton system is not able to work properly when energies present summing-out effects, the self-absorption correction factor obtained for n^a would be different compared with the one obtained for n. This explanation is consistent and it is according to some studies that have proven the possibility that $E_\gamma^{(1)}$ or $E_\gamma^{(2)}$ can be a low energy ($\leq$ 150 keV) in the case of 1120 keV [45]. Besides that, analogously to the explanation just given regarding the summing-out effects for 1120 keV, a similar situation could occur for 583 keV. In this latter case (583 keV), one of the possible values of $E_\gamma^{(1)}$ and $E_\gamma^{(2)}$ would be $E_\gamma^{(1)} = 57.766(5)$ keV (^{228}Ac) and $E_\gamma^{(2)} = 510.77(10)$. However, for 583 keV, the low energy (57.766(5) keV) is a gamma emission energy whose emission probability is very low (less than 0.50 %). Consequently, that low energy is unusually detected and, therefore, for 583 keV it is possible to correct n^a. Gamma emission energies and probabilities were taken from [36].

Despite not being possible to correct n^a in the case of 1120 keV, it is not a significant problem because this energy is usually used in order to determine ^{226}Ra, but this radionuclide can also be determined by many other energies.

3.3.1. Applications of the anti-Compton system: Calculations of detection limits

The anti-Compton system is used to reduce the Compton continuum, so this system results useful to improve the "detector sensibility", by doing the detection limit lower. This is possible because both the Compton continuum (B) and the lower limit of detection (L_D) are related by equations which have been taken from [46–48]. Therefore, making L_D lower, it could be helpful to be able to detect properly photons emitted by samples whose activities are very low, for example, water and vegetable samples.

Besides that, L_D is related to *MDA* (Minimum Detectable Activity) by another equation given below:

$$MDA = \frac{L_D}{\varepsilon t P_\gamma} \tag{8}$$

where ε, P_γ and t are the detector efficiency, the gamma emission probability and the measurement time, respectively. In our case, L_D values have been calculated at a significance level of 5 % for all the selected samples.

To study the influence of the anti-Compton system on the detection limit, six samples covering a wide range of densities and chemical compositions have been chosen: Ilmenite, Scale-1, IAEA-326, (RGU-1, RGTh-1, RGK-1) + 70 % PbS. Moreover, several E_γ values of interest have been selected throughout the energy region.

In Fig. 5, the MDA^a/MDA ratios have been plotted versus for the six samples mentioned above, where MDA^a and MDA are the minimum detectable activities when the anti-Compton system is on and off, respectively. In order to calculate the minimum detectable activities for both cases (MDA^a and MDA), the same measurement time was chosen for all the selected samples, being this of 172800 s (2 days). In that figure it is possible to note that the majority of the MDA^a/MDA ratios were ranged from 0.5 and 0.7 for all the samples and energies. It is necessary to clarify that at 186 keV, two cases were considered: With and without secular equilibrium between ^{238}U and ^{226}Ra. When secular equilibrium is not considered, the interference of ^{235}U (I_{235U}) on ^{226}Ra determination must be known. Thus, the interference can be estimated from the following equation:

$$I_{235U} = A_{235U} P_\gamma(235\text{U}) \varepsilon_{186keV} t = 0.02631 A_{238U} \varepsilon_{186keV} t \tag{9}$$

where A_{235U}, A_{238U} are the ^{235}U and ^{238}U activities, respectively, $P_\gamma(235U) = 0.572(5)$ at 186 keV, ε_{186keV} the efficiency value at 186 keV and t is the measurement time. Besides, it has been considered that $A_{235U}/A_{238U} = 0.046$ [49] as well as ^{238}U and ^{234}Th are in secular equilibrium. Therefore, since $A_{238U} = A_{234Th}$ and ^{234}Th can be determined, I_{235U} can be calculated.

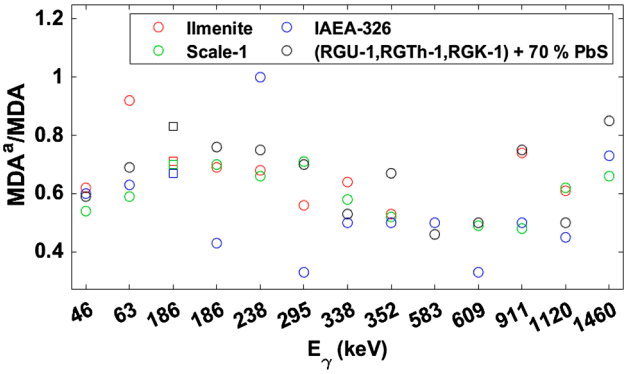

Fig. 5. Comparison between the *MDA* values obtained with and without anti-Compton system (MD/A^a and *MDA*, respectively) for several energies and types of samples. In the case of $E_\gamma = 186$ keV, the values of MDA^a/MDA corresponding to non-secular equilibrium between ^{238}U and ^{226}Ra have been shown by squares for each selected sample.

In the case of 186 keV without considering secular equilibrium between ^{238}U and ^{226}Ra, it is clearly seen in Fig. 5 that MDA^{α}/MDA values are higher compared with those values calculated when secular equilibrium between those two radionuclides is considered. This is very consistent since the minimum detectable activity is higher when the interference term (I) is introduced. In addition to Fig. 5, in Tables A.13 (see Supplementary Material) it is possible to find the values of MDA, MDA^{α} and MDA^{α}/MDA for all the samples and energies chosen in this section, as well as for the cases in which secular equilibrium between ^{238}U and ^{226}Ra has been and not been considered.

3.3.2. Applications of the anti-Compton system: Comparison between gamma and alpha-particle spectrometric techniques

In this Section, it has been carried out a comparison between gamma and alpha-particle spectrometric techniques in order to propose gamma spectrometry as an alternative analysis technique to alpha-particle spectrometry to determine certain natural long-lived radionuclides (^{226}Ra and ^{228}Ra).

^{226}Ra and ^{228}Ra are two radionuclides that are usually measured by alpha-particle spectrometry due to their environmental interest. However, their determinations by this spectrometric technique are very tedious, making necessary to use physical–chemical procedures in order to separate the radionuclides of interest from the original matrix. In addition to the complicated methods employed to determine ^{226}Ra and ^{228}Ra by alpha-particle spectrometry, these methods take a long time to be carried out, being approximately three weeks and six months in the cases of ^{226}Ra and ^{228}Ra, respectively. [26,27,50]

Therefore, given that using gamma spectrometry it is possible to determine ^{226}Ra and ^{228}Ra in a relatively simple and fast way, being the usual measurement times ranged from one to two days, this spectrometric technique is a very good alternative to alpha-particle spectrometry. However, this latter kind of spectrometry is characterized by having a very low detection limit for most samples, being its value approximately 5 mBq in the cases of ^{228,226}Ra and 1 mBq for the other natural long-lived radionuclides of interest such as ^{238}U, ^{228}Th and ^{210}Po. Consequently, it is necessary to reduce the detection limit for gamma spectrometry to reach the usual detection limit values in the case of alpha-particle spectrometry. For this, a possible procedure, which would allow us to get the desired detection limit values, would consist in concentrating the sample that is being tried to be measured by gamma spectrometry instead of alpha-particle spectrometry. In this case, a concentration factor (CF) would be necessary to calculate. In our case, given that the sample volume is always the same (4.94(15) cm^3), the CF factor would be defined by $CF = MDA^{\gamma}/MDA^{\alpha}$, where MDA^{γ} and MDA^{α} are the minimum detectable activities for samples measured by gamma spectrometry and alpha-particle spectrometry, respectively. Thus, by concentrating that sample, it would be possible to minimize the sample mass and, therefore, getting a lower L_D value. Furthermore, since the anti-Compton system is very helpful to reduce L_D values, it would be recommendable to be used in order to make the L_D reduction easier.

In this Section, it has been carried out a study on the calculations of CF values from a theoretical point of view. For this, the same samples that were chosen in the Section 3.3.1 have been selected, excepting RGK-1 + 70 % PbS. This sample was discarded because ^{40}K cannot be measured by alpha-particle spectrometry and, consequently, it is not possible to compare both techniques. Besides, in this Section, a sample of distilled water was chosen to study the CF values obtained in a liquid sample. On the other hand, apart from having chosen ^{226}Ra and ^{228}Ra in this Section to make that comparison, other radionuclides such as ^{210}Pb and ^{234}Th (being ^{210}Po and ^{238}U, respectively, the radionuclides used in the case of alpha-particle spectrometry), as well as ^{228}Th were also selected in order to achieve a more complete study. In Table 1 the CF^{α} and CF values, as well as the CF^{α}/CF ratios for all the samples previously mentioned can be found, where CF^{α} and CF are the concentration factors with the anti-Compton system on and off, respectively. In order to calculate the CF^{α} and CF factors for all the selected samples, a common measurement time (172800 s) was chosen.

In Table 1, it can be observed that the highest CF^{α} and CF values have been obtained in the cases of $E_{\gamma} = 46$, that is, for ^{210}Pb, occurring at $E_{\alpha} = 5304.38$ keV for ^{210}Po, where E_{α} is the alpha-particle emission energy. At 46 keV, CF^{α} values ranged from 25 to 1446, while CF values ranged from 42 to 2436 for distilled water and RGU-1 + 70 % PbS, respectively. On the other hand, the lowest CF^{α} and CF values have been observed for $E_{\gamma} = 911$ keV, corresponding to $E_{\alpha} = 5685.37$ keV in the case of alpha-particle spectrometry. For 911 keV, CF^{α} ranged from 3 to 20, whereas CF ranged from 4 to 41 for distilled water and Scale-1, respectively. As it could be expected the highest values of CF^{α} and CF are obtained for low E_{γ} because as E_{γ} decreases, the Compton continuum increases and, consequently, MDA and L_D also increase. It is worth noting that the lowest and highest values of CF^{α} and CF have been observed for samples whose activity concentrations are lower and higher, respectively, since MDA is higher as activity concentration of a sample increases.

Regarding 186 keV, both CF^{α} and CF values are higher when not considering secular equilibrium between ^{238}U and ^{226}Ra. This agrees with the results obtained in Section 3.3.1 because in absence of secular equilibrium, L_D and, therefore, MDA increase due to the interference term (I_{235U}). In this Section, the energy of 186 keV was selected to

Table 1
Comparison between the detection limits obtained for several radionuclides (energies) by alpha and gamma spectrometry techniques (RN^{γ} (E_{γ}) and RN^{α} (E_{α}), respectively), where CF ^{a} and CF are the concentration factors when the anti-Compton system is switched on and off, respectively, and $CF' = CF^{a}/CF$.

		Ilmenite			Scale-1			IAEA-326			(RGU-1, RGTh-1) + 70 % PbS			Distilled water		
RN^{γ} ($RN^{i\pm}$)	E_{γ} (keV) (E_{α} (keV))	CF	CF ^{a}	CF'	CF	CF ^{a}	CF'	CF	CF ^{a}	CF'	CF	CF ^{a}	CF'	CF	CF ^{a}	CF'
^{210}Pb (^{210}Po)	46.5 (5304.38)	494	307	0.62	549	297	0.54	103	61	0.59	2436	1446	0.59	42	25	0.60
^{234}Th (^{238}U)	63.29 (4198)	305	281	0.92	101	59	0.58	84	52	0.62	1197	828	0.69	41	22	0.54
^{226}Ra (^{226}Ra)	186.2 (4784.34) (No sec. eq.)	53	38	0.72	128	89	0.70	25	16	0.64	166	138	0.83	17	9	0.53
	186.2 (4784.34) (Sec. eq.)	29	20	0.69	73	51	0.70	14	7	0.50	93	70	0.75	9	5	0.56
^{212}Pb (^{228}Th)	238.64 (5423.15)	20	14	0.70	50	33	0.66	10	5	0.50	41	29	0.71	8	3	0.38
^{228}Ac (^{224}Ra)	911.07 (5685.37)	12	9	0.75	41	20	0.49	8	4	0.50	15	12	0.80	4	3	0.75

determine ^{226}Ra in order to make the calculations of possible ^{222}Rn losses unnecessary in the chosen samples. On the other hand, from Table 1 it is also possible to observe a significant reduction in *CF* when using the anti-Compton system leading to CF^{a}/CF ratios ranging between 0.5 and 0.7 for most samples and energies.

3.4. Validations of the methodology to calibrate in efficiency: Internal and external validation procedures

In order to test the validity of the methodology followed in this work to calibrate in efficiency, two kinds of validation procedures have been carried out: Internal and external validation procedures.

3.4.1. Internal validation procedure

In this validation, Phosphate Rock (PR-1) was mixed with six different proportions of PbS (0, 20, 40, 60, 70 and 80 %), increasing the PR-1 density and ⟨Z⟩. PR-1 was selected for this validation because this sample contains all the radionuclides of interest that belong to the ^{238}U-series as well as its chemical composition is very well known.

Five aliquots of PR-1 and PbS mixtures were measured by another detector (XtRa: Coaxial Extended Energy Range HPGe Detector), whose calibration in efficiency has already been tested, to give a reference value for activity concentrations (see Tables A.14 in Supplementary Material). The radionuclide reference activity concentrations were determined for the main gamma emission energies belonging to the ^{238}U-series, that is, 46 keV, 63 keV, 186 keV, 295 keV, 352 keV, 609 keV and 1120 keV. Once these reference activity concentrations were calculated for those two samples mentioned, the six mixtures of PR-1 and PbS, previously mentioned, were measured by the well-type detector. Then, by Eq. (2), it was possible to calculate the experimental efficiency values for all the energies and sample mixtures mentioned above. These experimental values, which have been obtained using the reference activities calculated by the XtRa calibration, let us call by ε_{Well}^{exp}. Therefore, ε_{Well}^{exp} allows us to differentiate that kind of efficiency from the efficiency values obtained by the well-type detector calibration, which let us call by ε_{Well}. Besides, the ε_{Well} values were calculated by the three functions proposed in Section 3.2 (*Function-i*, where $i = 1, 2, 3$), and, therefore, obtaining $\varepsilon_{Well}^{(1)}$, $\varepsilon_{Well}^{(2)}$ and $\varepsilon_{Well}^{(3)}$, respectively, for the efficiency values in the case of the well-type detector. In this way, it was possible to compare the ε_{Well}^{exp} values with the three functions proposed in Section 3.2.

In Fig. 6, $\varepsilon_{Well}^{(i)}$ values have been plotted versus ε_{Well}^{exp} for the seven energies and six samples mixtures mentioned above, showing six efficiency values for each E_γ value. It is necessary to clarify that as the PbS proportion increases, the efficiency value decreases both for ε_{Well}^{exp} and $\varepsilon_{Well}^{(i)}$. Therefore, taking this into account, in Fig. 6 it is perfectly possible to distinguish between the efficiency values obtained for each PbS proportion.

On the other hand, in Fig. 6 it is possible to find plotted the fittings done of $\varepsilon_{Well}^{(i)}$ versus ε_{Well}^{exp}, which have been carried out by $\varepsilon_{fit}^{(i)}$ functions. This kind of fitting was done in order to make the comparison between $\varepsilon_{Well}^{(i)}$ versus ε_{Well}^{exp} easier. Besides, two cases have been considered: ideal and real cases. The equations employed for the ideal and real fittings were $\varepsilon_{fit}^{(i)} = \varepsilon_{Well}^{exp}$ and $\varepsilon_{fit}^{(i)} = a + b\ \varepsilon_{Well}^{exp}$, respectively, being a and b the parameters resulted from the non-ideal fitting. Thus, it has been observed that the efficiency values given by $\varepsilon_{Well}^{(1)}$ were more similar to the ones obtained by ε_{Well}^{exp} in comparison with the other cases ($\varepsilon_{Well}^{(2)}$ and $\varepsilon_{Well}^{(3)}$). This is consistent since the reference activity concentration values of PR-1 and PbS (see Tables A.14 in Supplementary Material), which were used to obtain ε_{Well}^{exp}, were calculated using a self-absorption correction factor whose behavior is analogous to the one used in the case of the well-type detector (see [37,51] for further information about the self-absorption correction factor employed for XtRa detector).

Besides that, in Fig. 6 it can also be found the relative average residues for the three $\varepsilon_{fit}^{(i)}$ fitting functions corresponding to $\varepsilon_{Well}^{(i)}$ values. Thus, two types of relative average residues have been shown for the fittings done of $\varepsilon_{Well}^{(i)}$ values, $\langle Res \rangle_{\text{ideal}}$ and $\langle Res \rangle_{\text{fit}}$, which are related to

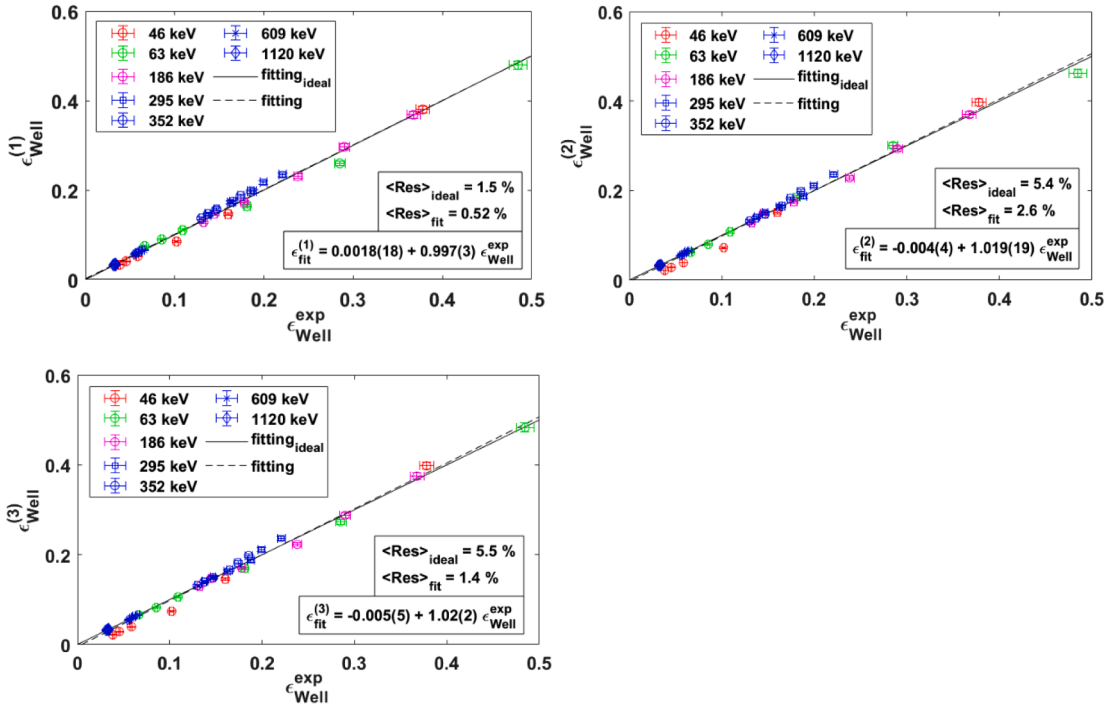

Fig. 6. Internal validation procedure carried out using a phosphate rock sample (PR-1) mixed with different proportions of PbS. This validation was done for three types of fitting functions ($\varepsilon_{\text{fit}}^{(i)}$, being "i" = 1, 2, 3), which were obtained after fitting $\varepsilon_{Well}^{(i)}$ vs ε_{Well}^{exp}. Besides, the relative average residues were calculated considering both the fittings done by the ideal and real $\varepsilon_{\text{fit}}^{(i)}$ functions ($\langle Res \rangle_{\text{ideal}}$ and $\langle Res \rangle_{\text{fit}}$, respectively).

the ideal and real fittings done by $\varepsilon_{fit}^{(i)}$, respectively. Therefore, it is easy to note that the residues resulted from $\varepsilon_{fit}^{(1)}$ fittings were lower for both cases ($\langle Res\rangle_{\text{ideal}} = 1.5$ % and $\langle Res\rangle_{\text{fit}} = 0.52$ %) in comparison with the ones obtained by $\varepsilon_{fit}^{(2)}$ and $\varepsilon_{fit}^{(3)}$ functions, where those residues were 5.4 % and 2.6 % ($\varepsilon_{fit}^{(2)}$) and 5.5 % and 1.4 % ($\varepsilon_{fit}^{(3)}$) for $\langle Res\rangle_{\text{ideal}}$ and $\langle Res\rangle_{\text{fit}}$, respectively. This agrees with the explanation previously given regarding the similarity between the self-absorption correction factors used in the cases of XtRa and well-type detectors. Taking the results obtained by the three kinds of *Function-i*, it is easy to note that the internal validation has been really good for the three cases.

In this Section, the external validation for the methodology of calibration in efficiency has been carried out. The samples selected for the validation were IAEA-326, PR-2 and RGK-1.

In Table 2, it is possible to see the z_{score} values resulted from the comparison made between activity concentration values calculated through the well-type detector calibration, having employed for it the *Function-1*, which was analyzed in Section 3.2, as well as Eq. (2), and the values of reference activity concentrations given for certified real samples. Regarding the z_{score} equation, which was used in order to do this validation, it is given by the following mathematical expression:

$$z_{score} = \frac{a - a_r}{\sqrt{\sigma_a^2 + \sigma_{a_r}^2}} \tag{10}$$

where a_r (σ_{a_r}) and a (σ_a) are the reference and calculated activity concentration values (and uncertainties at 1 sigma level), respectively. Besides, $-2 \leq z_{score} \leq 2$ is the range for which a calculation is considered good.

Moreover, in Table 2 it is also possible to find two values of activity concentrations for ^{226}Ra calculated at 186 keV: With and without considering secular equilibrium between ^{238}U and ^{226}Ra. Thus, in the former case, an equivalent probability has been obtained, P_γ^*, where $P_\gamma^* = P_\gamma(^{226}\text{Ra}) + {}^{235}\text{U}/{}^{238}\text{U}\ P_\gamma(^{235}\text{U}) = 6.14(6)$ %, being $P_\gamma(^{226}\text{Ra}) = 3.51(6)$ % and $P_\gamma(^{235}\text{U}) = 57.2(5)$ % at 186 keV, and $^{235}\text{U}/^{238}\text{U} = 0.046$. On the other hand, in the latter case (non-secular equilibrium between ^{238}U and ^{226}Ra), it would be necessary to take Eq. (2) considering the interference term (I_{235U}), which was defined in Eq. (9).

In Table 2 the z_{score} values for IAEA-326, PR-2 and RGK-1 have been shown. Regarding the IAEA-326 sample, all the $|z_{score}|$ values were less than 2, being the majority of them less than 1. In the case of PR-2 sample, a very good agreement between reference and calculated activity concentrations was obtained, where all the $|z_{score}|$ values were less than 1.5. Finally, for RGK-1 sample, a z_{score} value of 0.6 was obtained. Therefore, according to the external validation for all the selected samples and energies it is possible to infer a good agreement between the activity concentrations obtained through the method proposed in this work and the certified values.

On the other hand, since the self-absorption correction factor given by Eq. (3) does not work properly in the case of high-density samples with high values of ⟨Z⟩ (compared with the ⟨Z⟩ value of a soil, which is approximately 10.6), below it has been shown a study on the z_{score} values obtained for samples whose density and ⟨Z⟩ have been varied. For this, PR-2 sample has been chosen and it has been mixed with different PbS proportions (PbS proportions were ranged from 0% to 67.5 %), getting PR-2 density and ⟨Z⟩ increase. Consequently, this study allows us to find out the interval of density and ⟨Z⟩ within which Eq. (3) works correctly. Given that the self-absorption effects are more relevant at low energies, the gamma emission energy of 63 keV (^{234}Th) has been chosen in order to do this study, having calculated the z_{score} value for each PbS proportion at this energy.

In Fig. 7 it is possible to find the z_{score} values resulted from the calculated activity concentrations at 63 keV for each mixture of PR-2 with PbS. In that figure, there is a clear z_{score} dependence on the proportion of PbS, where the z_{score} values were ranged from −0.24 to −4.9 for 0 % and 67.5 % of PbS, respectively. Besides, it is interesting to note that 37.5 % was the PbS proportion from which the $|z_{score}|$ values began to be greater than 2, being approximately 15 cm^2 the ηm value obtained in this case, where $\eta = 1.52$ cm^2 P_γ^*. Therefore, from that ηm value, the self-absorption correction factor given by Eq. (3) begins to provide

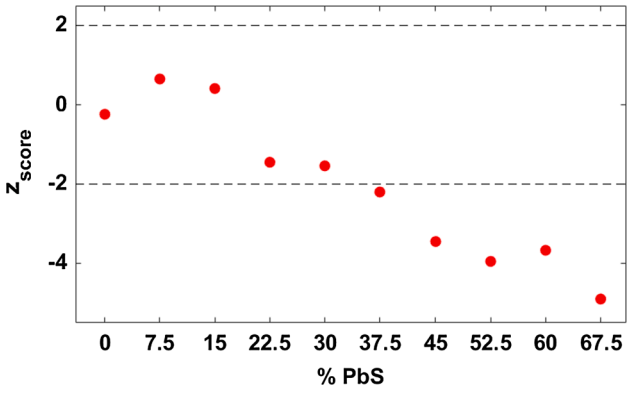

Fig. 7. Values of z_{score} resulted from the calculated activity concentrations at 63 keV for each mixture of PR-2 with PbS.

Table 2
External validation procedure done by the calculations of z_{score} values for several certified samples (IAEA-326, PR-2 and RGK-1). Besides, at 186 keV two cases have been considered: Without and with secular equilibrium between ^{238}U and ^{226}Ra (No sec. eq. and Sec. eq., respectively). Uncertainties given at 1 sigma level.

		IAEA-326			RGK-1			Phosphate Rock-2 (PR-2)		
RN	E_γ (keV)	a (Bq kg^{-1})	Reference	z_{score}	a (Bq kg^{-1})	Reference	z_{score}	a (Bq kg^{-1})	Reference	z_{score}
^{210}Pb	46.5	46(4)	53(5)	−1.1				1583(72)	1541(5)	0.6
^{234}Th	63.29	30(3)	29.4(1.7)	0.3				1525(68)		−0.2
^{226}Ra	186.2 (No sec. eq.)	41(3)	33(3)	1.8				1562(83)		0.3
	186.2 (Sec. eq.)	36(3)		0.9				1547(66)		0.1
^{214}Pb	295.21	26.4(1.5)		−1.8				1450(60)		−1.5
	351.92	26.9(1.3)		−1.7				1466(60)		−1.3
^{214}Bi	609.31	27.9(1.7)		−1.3				1483(62)		−0.9
	1120.2	26(3)		−1.5				1446(74)		−1.3
^{228}Ac	338.42	44(3)	40(2)	1.2						
	911.07	39(2)		−0.4						
^{212}Pb	238.64	39.6(1.7)	39.1(1.7)	0.2						
^{208}Tl	583.19	41(3)		0.5						
^{40}K	1460.83	568(25)	580(28)	−0.3	14359(606)	14000(200)	0.6			

improper corrections for self-absorption effects. This agrees with the study on different self-absorption correction functions carried out in Section 3.2.

3.5. A proposed method to determine ^{226}Ra under non-secular equilibrium with ^{222}Rn

In order to take advantage of the possibility of determining ^{226}Ra by its gamma emission energy (186 keV) as it was explained in Section 3.4.2, with or without considering that ^{238}U and ^{226}Ra are in secular equilibrium, some kinds of samples have selected in this Section, which are characterized by having ^{222}Rn losses. Therefore, for these types of samples, the ^{226}Ra determination proposed in this Section would be very helpful. The selected samples were IAEA-434, CSN-PG and RGU-1 standard dissolved in water (dissolved RGU-1), having been possible to dissolve this standard in water because of its previous digestion by using acids.

Regarding the samples that present a clear loss of ^{222}Rn, it is necessary to wait at least a month in order to ensure the secular equilibrium between ^{226}Ra and ^{222}Rn is reached. Consequently, the ^{226}Ra determination could not be carried out properly by its daughters (^{214}Pb and ^{214}Bi). Therefore, all the reasons previously exposed make necessary employ the proposed method in this Section to determine ^{226}Ra. (See [52–57] for further information about studies related to ^{222}Rn losses in different types of materials).

In Table 3 it has been shown the results of activity concentrations obtained for the three samples mentioned in this Section (IAEA-434, CSN-PG and dissolved RGU-1). Thus, it is easy to note that the ^{222}Rn losses were significant in the cases of IAEA-434 and CSN-PG (15(3) % and 11(2) %, respectively), which were measured without waiting for secular equilibrium between ^{226}Ra and ^{222}Rn being reached. On the other hand, in Table 3 it is also possible to check that the ^{222}Rn losses were even more relevant in the case of dissolved RGU-1, where the average ^{222}Rn losses obtained were 71(8) %. Consequently, taking these results into account, it has perfectly been proved the need for using the proposed method in this Section in order to carry out the ^{226}Ra determination.

4. Conclusions

In the present work, a novel methodology to carry out the calibration in efficiency of a well-type Ge detector has been developed. This methodology to calibrate in efficiency consisted on varying the density (mass) of the chosen calibration samples fixing their thicknesses and for each gamma emission energy of interest (E_γ). By this methodology, it has been possible to find a general function for the efficiency, which depends on ε_0 and f, where they are the efficiency value when the sample mass tends to zero and the self-absorption correction factor, respectively. Thus, it has been checked that ε_0 can be written as a function of E_γ.

On the other hand, regarding the self-absorption corrections, a comparative study between different correction functions (*Function-i*) has been carried out. This comparison was made considering the main gamma emissions from radionuclides belonging to ^{238}U- and ^{232}Th-series, and, specifically emphasis has been placed on studying the results obtained in the case of *Funtion-1*. This function is the most used in order to correct self-absorption effects for samples measured by a well-type detector. Thus, it has been proved that this function does not work properly when the $\langle Z \rangle$ value of a sample is very high in comparison with the $\langle Z \rangle$ value of a soil ($\sim$ 10.6).

Besides that, an in-depth study on advantages and disadvantages about using an anti-Compton system has been done. Thus, a variation of the counting rate when using an anti-Compton system (n^a) has been observed in comparison with the value when it is not used (n). This variation was noted for some specific energies: 583 keV, 609 keV and 1120 keV, which are characterized by presenting summing-out effects. Besides, it was possible to correct the n^a values for 583 keV and 609 keV, since it has been checked that the n^a/n ratio does not depend on the kind of sample. Only for 1120 keV, it was not possible to carry out that n^a correction due to the self-absorption effects that were present in one of the energies related to its summing-out effects. Then, it has been proved that an anti-Compton system can be very helpful to reduce the lower limit of detection (L_D), as well as to achieve the gamma spectrometry is a clear alternative to alpha-particle spectrometry for some radionuclides, ^{228,226}Ra, that are very complicated to be determined by the latter spectrometric technique.

Table 3
Study about ^{222}Rn losses carried out in phosphogypsum samples (IAEA-434 and CSN-PG), as well as in the dissolved RGU-1 sample. In the case of dissolved RGU-1, the reference value for activity concentration was 241.5(0.7) Bq kg^{-1}. Uncertainties given at 1 sigma level.

		IAEA-434				CSN-PG			
RN	E_γ (keV)	a (Bq kg^{-1})	Reference	z_{score}	^{222}Rn losses (%)	a (Bq kg^{-1})	Reference	z_{score}	^{222}Rn losses (%)
^{210}Pb	46.5	722(34)	680(29)	0.9		784(40)	781(15)	0.1	
^{234}Th	63.29	107(10)	120(6)	−1.1		52(13)	48.6(1.2)	0.3	
^{226}Ra	186.2 (No sec. eq.)	836(25)		1.4		661(24)		1.0	
	186.2 (Sec. eq.)	523(24)		−6.5		400(22)	634(13)	−9.2	
^{214}Pb	295.21	666(28)	780(31)	−2.7	15(5)	581(26)	580(13)	0.0	11(4)
	351.92	655(27)		−3.0	16(5)	543(23)		−1.4	12(4)
^{214}Bi	609.31	665(29)		−2.7	15(5)	566(27)	533(13)	1.1	11(4)
	1120.2	662(39)		−2.4	15(6)	566(42)		0.8	9(4)
					$<^{222}$Rn loss$>$ (%) = 15 (3)				$<^{222}$Rn loss$>$ (%) = 11 (2)

		Dissolved RGU-1			
RN	E_γ (keV)	a (Bq kg^{-1})	Reference	z_{score}	^{222}Rn losses (%)
^{210}Pb	46.5	227(10)	241.5(0.7)	−1.5	
^{234}Th	63.29	242(10)		0.1	
^{226}Ra	186.2 (No sec. eq.)	210(12)		−2.6	
	186.2 (Sec. eq.)	224(9)		−1.9	
^{214}Pb	295.21	74(3)		−52	70(7)
	351.92	75(3)		−53	69(7)
^{214}Bi	609.31	73(4)		−41	70(10)
	1120.2	64(10)		−18	74(27)
					$<^{222}$Rn loss$>$ (%) = 71(8)

Then, internal and external validation procedures of the methodology followed in this work have been carried out. Regarding the former kind of validation, a comparison between ε_{Well}^{exp} and $\varepsilon_{Well}^{(i)}$, being "i" ranged from 1 to 3, was made for several energies for PR-1 sample. Thus, $\varepsilon_{Well}^{(i)}$ values were calculated by each *Function-i*, observing that the best agreement between $\varepsilon_{Well}^{(i)}$ and ε_{Well}^{exp} was obtained in the case of *Function-1*. Consequently, the self-absorption correction factor given by *Function*-1, which is usually employed to correct self-absorption effects in the case of well-type detectors, has a very similar behavior compared with the one used for XtRa detectors. On the other hand, regarding the external validation, several certified real samples were selected and all the obtained $|z_{score}|$ values were less than 2, getting a great external validation. Furthermore, the PR-2 sample was mixed with different PbS proportions in order to demonstrate the validity range of *Function-1*, observing that the correction provided by this function is proper until approximately 37.5 % of PbS (where ηm 15 cm^2 for that PbS percentage, being $\eta = 1.52\ cm^2\ P_\gamma^*$).

Lastly, a study on ^{222}Rn losses in phosphogypsum and dissolved samples has been carried out in order to propose the ^{226}Ra determination be done by its gamma emission energy ($E_\gamma = 186$ keV), making it unnecessary to wait for the secular equilibrium between ^{226}Ra and ^{222}Rn be reached.

CRediT authorship contribution statement

A. Barba-Lobo: Conceptualization, Data curation, Formal analysis, Investigation, Methodology, Validation, Writing - original draft, Writing - review & editing. **E.G. San Miguel:** Conceptualization, Data curation, Formal analysis, Investigation, Methodology, Validation, Writing - original draft. **R.L. Lozano:** Conceptualization, Data curation, Formal analysis, Investigation, Methodology, Validation. **J.P. Bolívar:** Conceptualization, Data curation, Formal analysis, Investigation, Methodology, Supervision, Validation, Writing - original draft, Writing - review & editing.

Declaration of Competing Interest

The authors declare that they have no known competing financial interests or personal relationships that could have appeared to influence the work reported in this paper.

Acknowledgments

This research was partially funded by a project of the Regional Government of Andalusia "Basic processes regulating the fractionations and enrichments of natural radionuclides under acid mine drainage conditions" (Ref.: UHU-1255876), and a project of the Projects for Novel Principal Investigators "Quantitative study of the variables involved in the radon exhalation rate for granular solids; application to rafts of granular solid phosphogypsum" (Ref.: UHUPJ-00005-632). A.B.L. acknowledges support from funds provided by the Spanish Ministry of Science, Innovation and Universities' Research Agency and co-financing provided by the European Social Fund (ESF) and the Spanish National Youth Guarantee Implementation Plan under Contract No. PEJ2018-002676-A.

Appendix A. Supplementary material

Supplementary data to this article can be found online at https://doi.org/10.1016/j.measurement.2021.109561.

References

[1] M. Baskaran, Po-210 and Pb-210 as atmospheric tracers and global atmospheric Pb-210 fallout: a Review, J. Environ. Radioact. 102 (2011) 500–513, https://doi.org/10.1016/j.jenvrad.2010.10.007.
[2] T.M. Church, M.M. Sarin, U- and Th-Series Nuclides in the Atmosphere: Supply, Exchange, Scavenging and Applications to Aquatic Processes, Radioact. Environ. 13 (2008) 11–47, https://doi.org/10.1016/S1569-4860(07)00002-2.
[3] E.G. San Miguel, J.P. Pérez-Moreno, J.P. Bolívar, R. García-Tenorio, J.E. Martín, ^{210}Pb determination by gamma spectrometry in voluminal samples (cylindrical geometry), Nucl. Instrum. Methods Phys. Res. A 493 (2002) 111–120, https://doi.org/10.1016/S0168-9002(02)01415-8.
[4] E.G. San Miguel, J.P. Pérez-Moreno, J.P. Bolívar, R. García-Tenorio, A semi-empirical approach for determination of low-energy gamma-emmiters in sediment samples with coaxial Ge-detectors, Appl. Radiat. Isot. 61 (2004) 361–366, https://doi.org/10.1016/j.apradiso.2004.03.009.
[5] L. Barbero, M.J. Gázquez, J.P. Bolívar, M. Casas-Ruíz, A. Hierro, M. Baskaran, M. E. Ketterer, Mobility of Po and U-isotopes under acid mine drainage conditions: an experimental approach with samples from Río Tinto area (SW Spain), J. Environ. Radioact. 138 (2014) 384–389, https://doi.org/10.1016/j.jenvrad.2013.11.004.
[6] M. Blasco, M.J. Gázquez, S.M. Pérez-Moreno, J.A. Grande, T. Valente, M. Santisteban, M.L. de la Torre, J.P. Bolívar, Polonium behaviour in reservoirs potentially affected by acid mine drainage (AMD) in the Iberian Pyrite Belt (SW of Spain), J. Environ. Radioact. 152 (2016) 60–69, https://doi.org/10.1016/j.jenvrad.2015.11.008.
[7] M.J. Gázquez, J. Mantero, F. Mosqueda, J.P. Bolívar, R. García-Tenorio, Radioactive characterization of leachates and efflorescences in the neighbouring areas of a phosphogypsum disposal site as a preliminary step before its restoration, J. Environ. Radioact. 137 (2014) 79–87, https://doi.org/10.1016/j.jenvrad.2014.06.025.
[8] A. Hierro, M. Olías, C.R. Cánovas, J.E. Martín, J.P. Bolívar, Trace metal partitioning over a tidal cycle in an estuary affected by acid mine drainage (Tinto estuary, SW Spain), Sci. Total Environ. 497 (498) (2014) 18–28, https://doi.org/10.1016/j.scitotenv.2014.07.070.
[9] C.J. Luque, F. Vaca, A. García-Trapote, A. Hierro, J.P. Bolívar, E.M. Castellanos, Radionuclides transfer into halophytes growing in tidal salt marshes from the Southwest of Spain, J. Environ. Radioact. 150 (2015) 179–188, https://doi.org/10.1016/j.jenvrad.2015.08.002.
[10] V. Spasic-Jokic, L. Zupunski, I. Zupunski, Measurement uncertainty estimation of health risk from exposure to natural radionuclides in soil, Measurement 46 (2013) 2376–2383, https://doi.org/10.1016/j.measurement.2013.04.019.
[11] European Commission, Council Directive 2013/59/Euratom of 5 December 2013. Laying down basic safety standards for protection against the dangers arising from exposure to ionising radiation, 1983, https://ec.europa.eu/energy/sites/ener/files/rp_188.pdf.
[12] Z. Ahmed, In-Situ object calibration software (ISOCS) technique for ^{235}U mass verification, Measurement 145 (2019) 648–650, https://doi.org/10.1016/j.measurement.2019.05.058.
[13] E.E. Belgin, G.A. Aycik, Derivation of an efficiency-calibration simulation for a well-type HPGe detector using the Monte Carlo approach and analytical techniques, Radiat. Meas. 73 (2015) 36–45, https://doi.org/10.1016/j.radmeas.2014.10.003.
[14] F. Bochud, C.J. Bailat, T. Buchillier, F. Byrde, E. Schmid, J.-P. Laedermann, Simple Monte-Carlo method to calibrate well-type HPGe detectors, Nucl. Instrum. Methods Phys. Res. A 569 (2006) 790–795, https://doi.org/10.1016/j.nima.2006.09.040.
[15] J.-M. Laborie, G.L. Petit, D. Abt, M. Girard, Monte Carlo calculation of the efficiency response of a low-background well-type HPGe detector, Nucl. Instrum. Methods Phys. Res. A 479 (2002) 618–630, https://doi.org/10.1016/S0168-9002(01)00942-1.
[16] M.R. Zare, M. Kamali, Z. Omidi, M. Fallahi-Kapourchali, Designing and producing large-volume liquid gamma-ray standard sources for low radioactive pollution measurements of seawater samples by comparison between experimental and simulation results, Measurement 90 (2016) 412–417, https://doi.org/10.1016/j.measurement.2016.04.065.
[17] A. Barba-Lobo, F. Mosqueda, J.P. Bolívar, A general function for determining mass attenuation coefficients to correct self-absorption effects in samples measured by gamma spectrometry, Radiat. Phys. Chem. 179 (2021), 109247, https://doi.org/10.1016/j.radphyschem.2020.109247.
[18] M. Bonczyk, Determination of ^{210}Pb concentration in NORM waste – An application of the transmission method for self-attenuation corrections for gamma-ray spectrometry, Radiat. Phys. Chem. 148 (2018) 1–4, https://doi.org/10.1016/j.radphyschem.2018.02.011.
[19] J. Carrazana, N. Cornejo, M. Jurado, E. Capote, The effect of source chemical composition on the self-attenuation corrections for low-energy gamma-rays in soil samples, Appl. Radiat. Isot. 68 (2010) 360–363, https://doi.org/10.1016/j.apradiso.2009.10.013.
[20] M. Długosz-Lisiecka, M. Ziomek, Direct determination of radionuclides in building materials with self-absorption correction for the 63 and 186 keV γ-energy lines, J. Environ. Radioact. 150 (2015) 44–48, https://doi.org/10.1016/j.jenvrad.2015.07.018.
[21] P. Jodłowski, Self-absorption correction in gamma-ray spectrometry of environmental samples – an overview of methods and correction values obtained for the selected geometries, Nukleonika 51 (2006) 21-25, https://www.nukleonika.pl/www/back/full/vol51_2006/v51s2p21f.pdf.

[22] F. Martínez-Ruiz, E. Borrego, E.G. San Miguel, J.P. Bolívar, An efficiency calibration for 210Pb and 7Be measurements by gamma-ray spectrometry in atmospheric filters, Nucl. Instrum. Methods Phys. Res. A 580 (2007) 663-666, https://doi.org/10.1016/j.nima.2007.05.117.
[23] M.L. Montes, M.G. Rizzoto, J. Juri-Ayub, R. Torres-Astorga, M.A. Taylor, An alternative methodology to determine 210Pb activity soil profiles, J. Environ. Radioact. 208/209 (2019) 105998, https://doi.org/10.1016/j.jenvrad.2019.105998.
[24] J.A. Suárez-Navarro, A.M. Moreno-Reyes, C. Gascó, M.M. Alonso, F. Puertas, Gamma spectrometry and LabSOCS-calculated efficiency in the radiological characterisation of quadrangular and cubic specimens of hardened portland cement paste, Radiat. Phys. Chem. 171 (2020), 108709, https://doi.org/10.1016/j.radphyschem.2020.108709.
[25] P.G. Appleby, N. Richardson, P.J. Nolan, Self-absorption corrections for well-type germanium detectors, Nucl. Instrum. Methods Phys. Res. B 71 (1992) 228–233, https://doi.org/10.1016/0168-583X(92)95328-O.
[26] S.M. Pérez-Moreno, M.J. Gázquez, M. Casas-Ruiz, E.G. San Miguel, J.P. Bolívar, An improved method for radium-isotopes quartet determination by alpha-particle spectrometry by using 225Ra (229Th) as isotopic tracer, J. Environ. Radioact. 196 (2019) 113-124, https://doi.org/10.1016/j.jenvrad.2018.11.007.
[27] R. Thomas, J. Mantero, S.M. Pérez-Moreno, C. Ruiz-Canovas, I. Vioque, M. Isaksson, E. Forssell-Aronsson, E. Holm, R. García-Tenorio, 226Ra, 210Po and lead isotopes in a pit lake water profile in Sweden, J. Environ. Radioact. 223/224 (2020) 106384, https://doi.org/10.1016/j.jenvrad.2020.106384.
[28] P. Roos, Analysis of radionuclides using ICP-MS, Radioact. Environ. 11 (2008) 295–330, https://doi.org/10.1016/S1569-4860(07)11009-3.
[29] G. Wallner, R. Wagner, C. Katzlberger, Natural radionuclides in Austrian mineral water and their sequential measurement by fast methods, J. Environ. Radioact. 99 (2008) 1090–1094, https://doi.org/10.1016/j.jenvrad.2007.12.021.
[30] X. Hou, Liquid scintillation counting for determination of radionuclides in environmental and nuclear application, J. Radioanal. Nucl. Chem. 318 (2018) 1597-1628, https://link.springer.com/article/10.1007/s10967-018-6258-6.
[31] X. Hou, P. Roos, Critical comparison of radiometric and mass spectrometric methods for the determination of radionuclides in environmental, biological and nuclear waste samples, Anal. Chim. Acta 608 (2008) 105–139, https://doi.org/10.1016/j.aca.2007.12.012.
[32] J.H. Zaidi, M. Arif, S. Ahmad, I. Fatima, I.H. Qureshi, Determination of natural radioactivity in building materials used in the Rawalpindi/Islamabad area by γ-ray spectrometry and instrumental neutron activation analysis, Appl. Radiat. Isot. 51 (1999) 559–564, https://doi.org/10.1016/S0969-8043(99)00073-1.
[33] S. Landsberger, R. Kapsimalis, Comparison of neutron activation analysis techniques for the determination of uranium concentrations in geological and environmental materials, J. Environ. Radioact. 117 (2013) 41–44, https://doi.org/10.1016/j.jenvrad.2011.08.014.
[34] IAEA, Preparation of gamma-ray spectrometry reference materials RGU-1, RGTh-1 and RGK-1, 1987, https://nucleus.iaea.org/sites/ReferenceMaterials/Shared%20Documents/ReferenceMaterials/Radionuclides/IAEA-RGTh-1/rl_148.pdf.
[35] IAEA, Reference materials, 2020, https://nucleus.iaea.org/sites/ReferenceMaterials/Pages/Index-for-Radionuclides.aspx.
[36] The Lund/LBNL nuclear data search, 1999, http://nucleardata.nuclear.lu.se/toi/radSearch.asp.
[37] J. Mantero, M.J. Gázquez, S. Hurtado, J.P. Bolívar, R. García-Tenorio, Application of gamma-ray spectrometry in a NORM industry for its radiometrical characterization, Radiat. Phys. Chem. 116 (2015) 78–81, https://doi.org/10.1016/j.radphyschem.2015.02.018.
[38] NIST Standard Reference Database 126 (2004), https://physics.nist.gov/PhysRefData/XrayMassCoef/tab3.html.
[39] G. Gilmore, J. Hemingway, Practical gamma-ray spectrometry, John Wiley & Sons, Chichester, 1995, https://doi.org/10.1002/rcm.1290091227.
[40] A. Tedjani, C. Mavon, A. Belafrites, D. Degrelle, D. Boumala, D. Rius, J.E. Groetz, Well GeHP detector calibration for environmental measurements using reference materials, Nucl. Instrum. Methods Phys. Res. A 838 (2016) 12–17, https://doi.org/10.1016/j.nima.2016.09.022.
[41] Y. Venegas-Argumedo, M.E. Montero-Cabrera, True coincidence summing corrections for an extended energy range HPGe detector, AIP Conf. Proc. 1671 (2015), 030004, https://doi.org/10.1063/1.4927193.
[42] MATLAB (2021), https://es.mathworks.com/help/optim/ug/equation-solving-algorithms.html?lang=en.
[43] J.-M. Laborie, G.L. Petit, D. Abt, M. Girard, Monte Carlo calculation of the efficiency calibration curve and coincidence-summing corrections in low-level gamma-ray spectrometry using well-type HPGe detectors, Appl. Radiat. Isot. 53 (2000) 57–62, https://doi.org/10.1016/S0969-8043(00)00114-7.
[44] S.-L. Wang, T. Bai, J.-L. Fan, Y. Fan, Q.-L. Shi, Y.-Z. Chang, Efficiency calibration and coincidence summing effect correction of well-type HPGe detector, Nucl. Electron. Detection Technol. 28 (2008) 4810485, https://inis.iaea.org/search/search.aspx?orig_q=RN:41053533.
[45] IND04-MetroMetal, Ionising radiation metrology for the metallurgical industry: Procedural guide for calculation of true coincidence summing correction factors for samples in metallurgical industry (2013), http://projects.ciemat.es/documents/16805/0/IND-04-12.pdf/e5d1682f-fbdb-42df-a0a3-9c573e8de3f2.
[46] J.P. Bolívar, Aplicaciones de la espectrometría gamma y alfa al estudio del impacto radiactivo producido por industrias no nucleares, Ph.D. Thesis (1995), University of Seville, https://idus.us.es/handle/11441/15757;jsessionid=42BB498B6CEA3B51479807DD80A23830?
[47] Ll.A. Currie, Limits for qualitative detection and quantitative determination. Application to radiochemistry, Anal. Chem. 40 (1968) 586-593, https://doi.org/10.1021/ac60259a007.
[48] K. Debertin, R.G. Helmer, Gamma- and X-ray spectrometry with semiconductor detectors, Elsevier, Amsterdam (1988), https://inis.iaea.org/search/search.aspx?orig_q=RN:20046286.
[49] A.R. Agha, S.A. El-Mongy, A.E. Kandel, Assay of uranium isotopic ratios 234U/238U, 235U/238U in bottom sediment samples using destructive and non destructive techniques (Nasser Lake), Proceedings of the eighth Nuclear and Particle Physics Conference (NUPPAC-2011) 43 (2011) 221-229, https://inis.iaea.org/search/search.aspx?orig_q=RN:43099476.
[50] F.V. Clulow, N.K. Davé, T.P. Lim, R. Avadhanula, Radium-226 in water, sediments, and fish from lakes near the city of Elliot Lake, Ontario, Canada, Environ. Pollut. 99 (1998) 13–28, https://doi.org/10.1016/S0269-7491(97)00176-0.
[51] J.P. Pérez-Moreno, E.G. San Miguel, J.P. Bolívar, J.L. Aguado, A comprehensive calibration method of Ge detectors for low-level gamma-spectrometry measurements, Nucl. Instrum. Methods Phys. Res. A 491 (2002) 152–162, https://doi.org/10.1016/S0168-9002(02)01165-8.
[52] J.C. Scholten, I. Osvath, M. Khanh-Pham, ^{226}Ra measurements through gamma spectrometric counting of radon progenies: How significant is the loss of radon? Mar. Chem. 156 (2013) 146–152, https://doi.org/10.1016/j.marchem.2013.03.001.
[53] F. Lamonaca, V. Nastro, A. Nastro, D. Grimaldi, Monitoring of indoor radon pollution, Measurement 47 (2014) 228–233, https://doi.org/10.1016/j.measurement.2013.08.058.
[54] P. Kuzmanović, N. Todorović, S. Forkapić, L.F. Petrović, J. Knežević, J. Nikolov, B. Miljević, Radiological characterization of phosphogypsum produced in Serbia, Radiat. Phys. Chem. 166 (2020), 108463, https://doi.org/10.1016/j.radphyschem.2019.108463.
[55] J.H. Hightower, J.E. Watson, 222Rn in water: a study of two sample collection methods, effects of mailing samples, and temporal variation of concentrations in North Carolina groundwater, Health Phys. 69 (1995) 219–226, https://doi.org/10.1097/00004032-199508000-00006.
[56] R.R. Benke, K.J. Kearfott, Accounting for ^{222}Rn loss during oven drying for the immediate laboratory gamma-ray spectroscopy of collected soil samples, Appl. Radiat. Isot. 52 (2000) 271–287, https://doi.org/10.1016/S0969-8043(99)00144-X.
[57] K. Tudyka, F. Pawelczyk, A. Michczyński, Bias arising from ^{222}Rn contamination in standardized methods for biobased content determination and a simple removal method, Measurement 167 (2021), 108263, https://doi.org/10.1016/j.measurement.2020.108263.